Phase Transformations in Iron-Nitride Compound Layers upon Low-Temperature Annealing: Diffusion Kinetics of Nitrogen in ε- and γ'-Iron Nitrides

T. LIAPINA, A. LEINEWEBER, and E.J. MITTEMEIJER

The ε/γ'-iron nitride (ε-Fe_3N_{1+x}, γ'-Fe_4N) compound double layers with thicknesses of about 10 μm were grown on pure α-Fe, by gas nitriding at 823 K, followed by quenching. The specimens were subsequently annealed at significantly lower temperatures, in the range of 613 to 693 K, for different periods of time. These heat treatments led to a redistribution of N, within the compound layer as well as between the compound layer and the adjacent ferrite, inducing thickness changes in the ε-and γ'-sublayers. The microstructure and sublayer-thickness changes were analyzed by light microscopy and X-ray diffraction (XRD). The experimentally observed time and temperature dependences of the layer-thickness changes were compared with the results obtained from numerical simulations, by adopting a model based on volume diffusion in the ε- and γ'-phases and on local equilibrium at the phase interfaces. In this manner, the intrinsic diffusion coefficient of N in the ε-phase and the integral diffusion coefficient of N in the γ'-phase were determined for the applied range of annealing temperatures.

I. INTRODUCTION

THE nitriding of iron and steel is of considerable technological importance, because it can make a pronounced improvement in the fatigue, the wear, and the corrosion resistance of these materials. One of the most important nitriding methods is the gas nitriding method,[1,2] which allows control of the chemical potential of nitrogen at the surface *via* the composition of the gas (NH_3-based) phase. Thus, the controlled formation of iron-nitride phases as compound layers on the surface of the (in most cases, ferritic) solid substrate is possible. In such layers, usually local equilibrium is assumed at the phase interfaces, *i.e.*, at the gas-solid interface, according to the chemical potential of the nitrogen in the gas atmosphere, and at the solid-solid interfaces, in accordance with the phase diagram (for pure Fe-N, refer to Figure 1).[3,4]*

*Single-phase iron-nitride specimens in equilibrium with a nitriding atmosphere can be generated by "through nitridin," starting from iron powder or thin iron foils.

By quenching to ambient temperature after nitriding, the nitrogen concentration-depth profile at the nitriding temperature can be retained. By slow cooling after nitriding, a method often employed in industry, the nitrogen concentration-depth profile may change, in association with changes in the (equilibrium) phase-boundary concentrations. These changes may lead to phase transformations in the compound layer[5] and, thus, to alterations in the microstructure of the compound layer. Information about processes occurring in the compound layer at temperatures below the nitriding temperature is scarce.

The present work reports a study of the annealing-induced redistribution of N in ε/γ'-iron nitride compound layers grown by gas nitriding on the surface of a thin plate of α-iron that had become saturated with nitrogen during the (sufficiently long) nitriding process. Annealing was performed in the temperature range of 613 to 693 K, which is well below the nitriding temperature of 823 K (Figure 1). The first results of such experiments performed by the present authors at an annealing temperature of 633 K revealed a "backward growth" of the γ'-sublayer at the cost of the ε-sublayer.[6] This effect can be qualitatively explained by the shift in the equilibrium N concentration in the ε-phase in contact with the γ'-phase to a higher value, upon lowering the temperature (*i.e.*, from the nitriding to the annealing temperature, as shown in Figure 1). Further work[7] showed that, for relatively high annealing temperatures, close to 690 K, significant diffusion through the γ'-sublayer occurs, even though the N concentration gradient across the γ'-layer is small. This N redistribution eventually led to a two-phase specimen ($\alpha + \gamma'$), in accordance with the Fe-N phase diagram and the gross-N content of the whole specimen (which contained slightly more nitrogen than that corresponding to the solubility limit of nitrogen in ferrite).

Until now, the kinetics of the N concentration profile development and phase (compound) formation was examined on the basis of the inward diffusion of nitrogen upon nitriding at temperatures above, for example, 770 K.[8,9] The exceptions are studies devoted both to the oxidation of iron-nitride compound layers at lower temperatures that also involve N redistribution processes,[10] and to the cooling-rate dependence of the microstructure of compound layers,[11,12] which, however, did not yield quantitative kinetic data. The type of annealing experiments employed in the current project allows the acquisition of kinetic data on N redistribution in iron nitrides at temperatures much lower than the typical nitriding

T. LIAPINA, Postdoctor, formerly with the Max Planck Institute for Metals Research, Heisenbergstraße 3, D-70569 Stuttgart, Germany, is with the Max Planck Institute for Steel Research GmbH, D-40237 Düsseldorf, Germany. A. LEINEWEBER is with the Max Planck Institute for Metals Research. Contact e-mail: a.leineweber@mf.mpg.de E.J. MITTEMEIJER, Director, Max Planck Institute for Metals Research, is Professor, Institute for Physical Metallurgy, University of Stuttgart, D-70569 Stuttgart, Germany.

Manuscript submitted April 13, 2005.

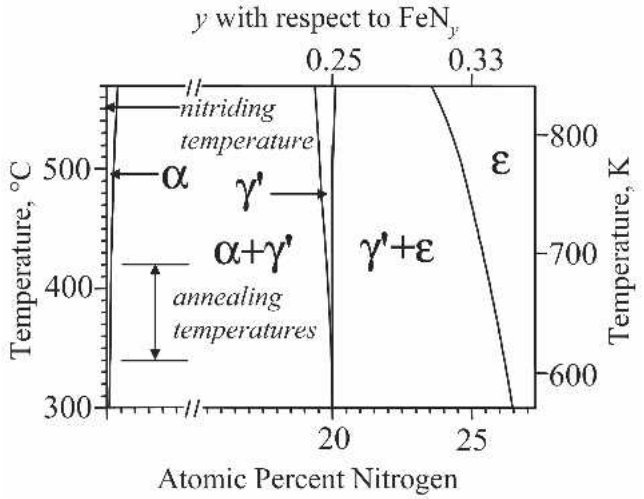

Fig. 1—Part of the Fe-N phase diagram. Note the interruption in the abscissa. The nitriding temperature and the range of annealing temperatures pertaining to this work have been indicated.

temperatures. Through these experiments, the present data, pertaining to a temperature range of 613 to 693 K, and evaluated in terms of the diffusion coefficients of N in the ε- and γ'-phases, can be compared with corresponding data obtained from high-temperature nitriding.

II. EXPERIMENTAL PROCEDURES

An iron (Alfa Aesar, 99.97 wt pct) cast rod was cold rolled to a plate about 1 mm in thickness. Before nitriding, a rectangular specimen (15 × 20 mm) cut from this plate was recrystallized for 1 hour at 980 K in vacuum and mechanically polished (final stage: 1-μm diamond).

Nitriding was performed in a vertical quartz-tube furnace in a 60 vol pct NH_3 (Matheson: 99.998 vol pct) and 40 vol pct H_2 (Hoek Loos: 99.999 vol pct) gas mixture, with a flow rate of 100 mL/min at 823 K for 5 hours. After nitriding, the specimen was quenched by dropping it into water flushed with N_2.

For each annealing temperature, a separate as-nitrided plate was subdivided into several rectangular pieces; each of these pieces was subjected to a heat treatment of different duration. As part of this process, the specimen was contained in an evacuated quartz tube. The annealing occurred in a salt bath (with a temperature accuracy within about 0.1 K) at five different temperatures (613, 633, 653, 673, and 693 K), followed by quenching in cold water without crushing the tube.

Optical microscopy on the as-nitrided and annealed specimens was performed with an Axiophot (Zeiss) microscope. To this end, embedded cross sections were ground, polished, and etched in 1 vol pct Nital that contained 0.1 vol pct HCl. For each specimen, 14 micrographs at laterally equidistantly distributed locations at the cross-sectional surface (in sample 7, close to each of both faces of the specimen) were recorded. The ε- and γ'-layer thicknesses were determined separately, using the program ImageTool (Version 3.0): the measured area of the layer was divided by the measured lateral length of the layer, in order to calculate the layer thickness; as a result, the effect of interface roughness is averaged out.

The X-ray diffraction (XRD) was performed with a PHILIPS* X'Pert MPD diffractometer, using Co K_α radiation and a graphite monochromator in the diffracted beam. On the sample surface, Si powder suspended in isopropanol was deposited, to serve as a standard. Diffraction data were recorded in the diffraction angle range of 30 deg $\leq 2\theta \leq$ 110 deg. The positions of the iron-nitride and silicon reflections were obtained by profile fitting, using pseudo-Voigt functions.[13] The 2θ scale was calibrated using the positions of the Si reflections. For each investigated specimen, lattice parameters of the ε-iron nitride were refined on the basis of the corrected diffraction angles of the same set of *hkl* reflections of the ε-phase.

*PHILIPS is a trademark of Philips Electronic Instruments Corp., Mahwah, NJ.

III. NITROGEN-REDISTRIBUTION PROCESSES IN ε/γ'-COMPOUND LAYERS

All the considerations about the N redistribution discussed here depart from the concentration-depth profile of the as-nitrided and quenched specimens (Figure 2, original profile) and satisfy the conservation of the overall number of N atoms in the compound layer. It is assumed that no nucleation of new phases occurs inside the ε- and γ'-sublayers (as observed under certain circumstances in References 11 and 12), but that phase transformations occur only at the already existing phase interfaces. Furthermore, the predictions set forth in Sections III and IV, for the direction of the changes in layer thicknesses, are only fully valid if the average N content of the ε-phase in the as-nitrided and quenched state, $y^{\varepsilon}_{\mathrm{av},0}$, is lower than the equilibrium N content of ε in contact with γ' at the annealing temperature, $y^{\varepsilon}_{\mathrm{eq}}$. This is ensured by the nitriding conditions described in Section II, and is in agreement with the experimental results obtained in this work.

At the phase interfaces, the N concentration in the as-nitrided and quenched specimens is supposed to comply with local equilibrium at the nitriding temperature.[3,8] For the ε-layer, the N content at the specimen surface (depth = 0) is indicated by $y^{\varepsilon}_{\mathrm{gas}/\varepsilon,0}$,** with values as obtained by the expressions given in Reference 14; the N content at the ε/γ'-interface at the depth $s_{\varepsilon,0}$ (as experimentally determined by optical microscopy) is indicated by $y^{\varepsilon}_{\varepsilon/\gamma',0}$, as obtained from the phase-boundary concentrations given in Reference 3. Between these boundary values, the N concentration-depth profile in the ε-sublayer is assumed to be linear; this is supported by experimental evidence given in Reference 3.

**Throughout the present article, the N contents of the ε- and γ'-iron nitrides are quantified by the ratio of the number of N and Fe atoms, y, as occurring in the formula FeN$_y$, recognizing the interstitial character of these iron nitrides.

The γ'-phase ranges from the depth $s_{\varepsilon,0}$ to $s_{\varepsilon,0} + s_{\gamma',0}$, where $s_{\gamma',0}$ is the γ'-sublayer thickness of the as-nitrided and quenched specimen, as determined by optical microscopy. The homogeneity range of the γ'-phase is sufficiently narrow to take the N concentration in the γ'-layer as constant at $y^{\gamma'} = 1/4$, for the mass balance considerations. The α-iron bulk substrate is saturated with N, after the nitriding process applied to the present samples. For the mass balance considerations, the nitrogen in the saturated ferritic bulk can be ignored.[6]

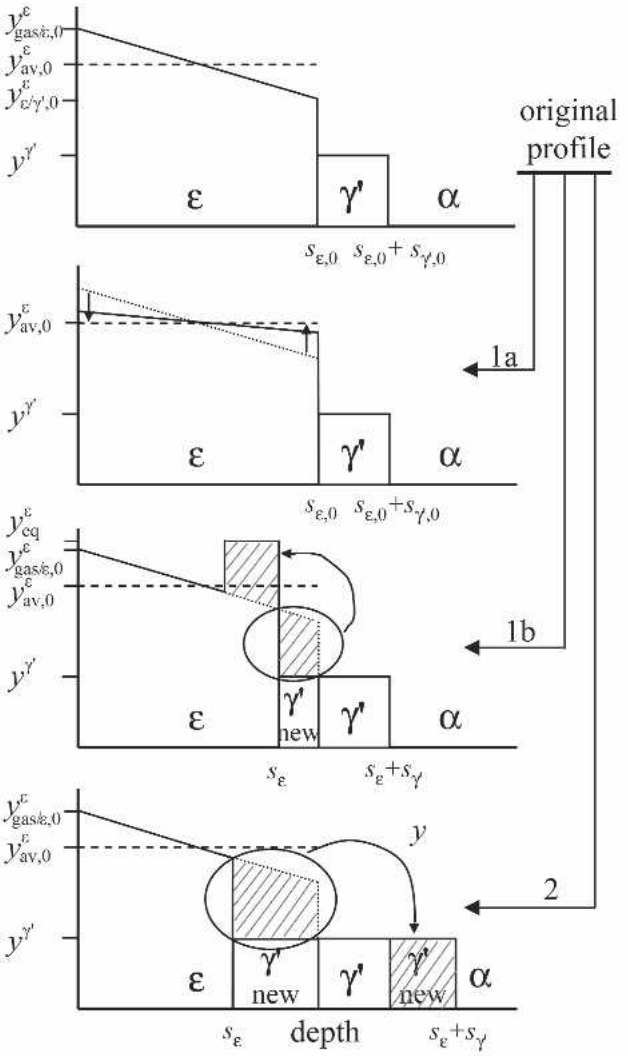

Fig. 2—Schematic illustration of the original N concentration-depth profile after nitriding, and the expected changes by different processes of nitrogen redistribution that may take place upon annealing below the nitriding temperature.

Upon annealing below the nitriding temperature, different subprocesses involving the compound layer of the as-nitrided specimens described earlier can be expected to occur (Figure 2).

(a) Process 1(a): The diffusion of N within the ε-phase, to level off the N concentration gradient, due to the difference between the chemical potentials at the gas/ε-and ε/γ'-interfaces. This leveling process alone would lead to a constant average N concentration, $y^{\varepsilon}_{\mathrm{av},0} = \left(y^{\varepsilon}_{\mathrm{gas}/\varepsilon,0} + y^{\varepsilon}_{\varepsilon/\gamma',0}\right)/2$, throughout the ε-layer. As indicated in the Appendix, this type of N redistribution inside the ε-phase does not significantly change its thickness (*i.e.*, the thickness change is much less than detectable by optical microscopy).

(b) Process 1(b): The backward growth of the γ'-layer at the cost of the ε-layer, to establish the temperature-decrease (nitriding temperature to annealing temperature)-induced change of the $\gamma' + \varepsilon/\varepsilon$-phase-boundary concentration in the ε-phase. This implies an increase in the N content in the ε/γ' interface-adjacent region in ε, up to the concentration in equilibrium with the γ'-phase at the annealing temperature, $y^{\varepsilon}_{\mathrm{eq}}$. For a small volume element of the ε-phase at the interface to the γ'-phase, the process can be described by the reaction scheme

$$\varepsilon\text{-FeN}_{y^{\varepsilon}_{\varepsilon/\gamma'}} \rightarrow \beta\gamma'\text{-FeN}_{1/4} + (1-\beta)\varepsilon\text{-FeN}_{y^{\varepsilon}_{\mathrm{eq}}} \qquad [1]$$

where

$$\beta = 4\left(y^{\varepsilon}_{\mathrm{eq}} - y^{\varepsilon}_{\varepsilon/\gamma'}\right)/\left(4y^{\varepsilon}_{\mathrm{eq}} - 1\right) \qquad [2]$$

with $y^{\varepsilon}_{\varepsilon/\gamma'}$ being the N content of the ε-phase at the ε/γ' interface (initially $y^{\varepsilon}_{\varepsilon/\gamma'} = y^{\varepsilon}_{\varepsilon/\gamma',0}$). In order to distribute the N originating from that part of the ε-phase that has transformed into γ'-phase over the remaining ε-phase, the diffusion of N in ε has to occur (as in Process 1(a), described earlier). If Processes 1(a) and 1(b) acted alone until completion, then the γ'-phase would grow until the whole remaining ε-phase has attained the composition $y^{\varepsilon}_{\mathrm{eq}}$. Calculations show that, for Processes 1(a) and 1(b), the overall double-layer thickness remains virtually constant (Section IV).

(c) Process 2: The diffusion of nitrogen through γ'-phase, leading to the formation of new γ'-phase. Although for the mass-balance considerations the γ'-phase is assumed to be stoichiometric ($y^{\gamma'} = 1/4$), a very small concentration gradient and, thus, a chemical potential gradient exists over its layer thickness; this implies a driving force by which N diffuses from the ε-phase through the γ'-layer and reacts with iron from the ferrite to form γ'-phase. Through this process, new γ' is formed, not only at the γ'/ε-interface, as for Process 1(b), but also at the α/γ'-interface:

$$\varepsilon\text{-FeN}_{y^{\varepsilon}_{\varepsilon/\gamma'}} + (4y^{\varepsilon}_{\varepsilon/\gamma'} - 1)\alpha\text{-Fe} \rightarrow \gamma'\text{-FeN}^{\gamma'/\varepsilon}_{1/4} + (4y^{\varepsilon}_{\varepsilon/\gamma'} - 1)\gamma'\text{-FeN}^{\alpha/\gamma'}_{1/4} \qquad [3]$$

If Process 2 proceeds until completion, the whole ε-layer will eventually be transformed into γ'-phase, leaving a single γ'-layer at the surface of the specimen. The specimen then represents the equilibrium $\alpha + \gamma'$ two-phase system, consistent with the phase diagram (Figure 1) and the gross-N content of the system, as described in Section I. In the course of Process 2, the (initially double-) layer thickness increases significantly, in contrast with Processes 1(a) and 1(b), as will be described in Section IV.

IV. LIMITING CASES OF NITROGEN REDISTRIBUTION

The N redistribution processes are accompanied by sublayer-thickness changes, from $s_{\gamma',0}$ to $s_{\gamma'}$ for the γ'-sublayer, and from $s_{\varepsilon,0}$ to s_{ε} for the ε-sublayer. Since the time-dependent evolutions of $s_{\gamma'}$ and s_{ε}, as determined by optical microscopy, provide the main tool in this work for tracing the kinetics of the N redistribution processes upon annealing, the sublayer thickness changes were analyzed quantitatively in detail.

In reality, all three described elementary processes of N redistribution, Processes 1(a), 1(b), and 2 (Section II), could be expected to occur simultaneously upon annealing at a temperature lower than the nitriding temperature. The limiting cases of N redistribution, according to these processes, can be described as follows.

(a) Limiting case ***A*** corresponds to the simultaneous occurrence of Processes 1(a) and 1(b). It starts from the concentration-depth profile of the as-nitrided state (original profile, Figure 2), characterized by the sublayer thicknesses $s_{\varepsilon,0}$ and $s_{\gamma',0}$ as well as by the average N content in the ε-phase $y^{\varepsilon}_{\mathrm{av},0}$. Upon annealing, s_ε decreases and $s_{\gamma'}$ increases, while saturation of the remaining ε-layer takes place in conjunction with N diffusion in the ε-layer. The ε-layer thickness, s_ε, and the average N content of the ε-layer, $y^{\varepsilon}_{\mathrm{av}}$, both as a function of the γ'-layer thickness, $s_{\gamma'}$, obey (also Reference 6)

$$s_\varepsilon(s_{\gamma'}) = \left(\frac{s_{\varepsilon,0}}{V^{\varepsilon}_{y^{\varepsilon}_{\mathrm{av},0}}} - \frac{s_{\gamma'} - s_{\gamma',0}}{V^{\gamma'}}\right) V^{\varepsilon}_{y^{\varepsilon}_{\mathrm{av}}} \qquad [4]$$

with

$$y^{\varepsilon}_{\mathrm{av}}(s_{\gamma'}) = \frac{4 s_{\varepsilon,0} V^{\gamma'} y^{\varepsilon}_{\mathrm{av},0} - V^{\varepsilon}_{y^{\varepsilon}_{\mathrm{av},0}} (s_{\gamma'} - s_{\gamma',0})}{4 s_{\varepsilon,0} V^{\gamma'} - 4 V^{\varepsilon}_{y^{\varepsilon}_{\mathrm{av},0}} (s_{\gamma'} - s_{\gamma',0})} \qquad [5]$$

where $V^{\gamma'}$ and V^{ε} are the volumes per iron atom of the γ'- and ε-phases (the Appendix provides more details). Equation [5] can be employed to estimate $y^{\varepsilon}_{\mathrm{av}}$ on the basis of the known parameters of the as-nitrided state ($s_{\varepsilon,0}$,$s_{\gamma',0}$,$y^{\varepsilon}_{\mathrm{av},0}$) and the measured value of the γ'-layer thickness ($s_{\gamma'}$). The average N content in the remaining ε-layer can also be determined from the measured value of the ε-layer thickness (s_ε) by iteratively solving*

*This is required, because $V^{\varepsilon}_{y^{\varepsilon}_{\mathrm{av}}}$ in the right part of Eqs. [6] and [8] depends slightly on $y^{\varepsilon}_{\mathrm{av}}$.

$$y^{\varepsilon}_{\mathrm{av}}(s_\varepsilon) = \frac{s_{\varepsilon,0} V^{\varepsilon}_{y^{\varepsilon}_{\mathrm{av}}} (4 y^{\varepsilon}_{\mathrm{av},0} - 1) + s_\varepsilon V^{\varepsilon}_{y^{\varepsilon}_{\mathrm{av},0}}}{4 s_\varepsilon V^{\varepsilon}_{y^{\varepsilon}_{\mathrm{av},0}}} \qquad [6]$$

Equations [5] and [6] are fully equivalent. However, it should be noted that, even if the limiting case ***A*** occurred, due to experimental inaccuracy, experimentally obtained values for s_ε and $s_{\gamma'}$ would lead to slightly different values of $y^{\varepsilon}_{\mathrm{av}}$, by application of Eqs. [5] and [6].

Limiting case ***A*** has been completed when the concentration in the whole ε-layer has become equal to $y^{\varepsilon}_{\mathrm{eq}}$, with the corresponding sublayer thickness values $s_{\varepsilon,A}$ and $s_{\gamma',A}$, as obtained by the insertion of $y^{\varepsilon}_{\mathrm{av}} = y^{\varepsilon}_{\mathrm{eq}}$ into Eq. [5], followed by insertion of $s_{\gamma',A}$ into Eq. [4];

(b) Limiting case ***B*** corresponds to the sole occurrence of Process 2, starting from the as-nitrided state (original profile, Figure 2). The N from the ε-phase close to the ε/γ'-interface is transported through the γ'-layer, leading to the formation of new γ' at the ε/γ'- and γ'/α-interfaces. For the case in which only Process 2 occurs, this redistribution of nitrogen does not change the original N concentration profile in the ε-phase, *i.e.*, limiting case ***B*** implies that N diffusion inside the ε-phase is negligible. For this case, the relation between the ε- and γ'-layer thicknesses is given by

$$s_\varepsilon(s_{\gamma'}) = \frac{V^{\varepsilon}_{y^{\varepsilon}_{\mathrm{av}}}}{y^{\varepsilon}_{\mathrm{av}}} \left(\frac{s_{\varepsilon,0} y^{\varepsilon}_{\mathrm{av},0}}{V^{\varepsilon}_{y^{\varepsilon}_{\mathrm{av},0}}} - \frac{(s_{\gamma'} - s_{\gamma',0})}{4 V^{\gamma'}}\right) \qquad [7]$$

The average content of N in the remaining ε-phase, $y^{\varepsilon}_{\mathrm{av}}$, can be obtained as a function of $s_{\gamma'}$ iteratively*

$$y^{\varepsilon}_{\mathrm{av}}(s_{\gamma'}) = \frac{\Delta y^{\varepsilon}_0 + 2 y^{\varepsilon}_{\mathrm{av},0}}{4} + \sqrt{\left(\frac{\Delta y^{\varepsilon}_0 + 2 y^{\varepsilon}_{\mathrm{av},0}}{4}\right)^2 - \frac{V^{\varepsilon}_{y^{\varepsilon}_{\mathrm{av}}} \Delta y^{\varepsilon}_0}{2 s_{\varepsilon,0}} \left(\frac{s_{\varepsilon,0} y^{\varepsilon}_{\mathrm{av},0}}{V^{\varepsilon}_{y^{\varepsilon}_{\mathrm{av},0}}} - \frac{(s_{\gamma'} - s_{\gamma',0})}{4 V^{\gamma'}}\right)} \qquad [8]$$

where $\Delta y^{\varepsilon}_0 = \left(y^{\varepsilon}_{\varepsilon/\mathrm{gas},0} - y^{\varepsilon}_{\varepsilon/\gamma',0}\right)$.

The averaged N content in the ε-layer $y^{\varepsilon}_{\mathrm{av}}$ as a function of s_ε is straightforwardly given by

$$y^{\varepsilon}_{\mathrm{av}}(s_\varepsilon) = y^{\varepsilon}_{\mathrm{av},0} + \frac{1}{2} \Delta y^{\varepsilon}_0 \left(\frac{s_{\varepsilon,0} - s_\varepsilon}{s_{\varepsilon,0}}\right) \qquad [9]$$

Boundary process ***B*** is completed when the whole ε-layer has been consumed and a single γ'-layer on top of the ferritic substrate is present with the thickness

$$s_{\gamma',B} = s_{\gamma',0} + \frac{4 s_{\varepsilon,0} y^{\varepsilon}_{\mathrm{av},0} V^{\gamma'}}{V^{\varepsilon}_{y^{\varepsilon}_{\mathrm{av},0}}} \qquad [10]$$

(c) Limiting case ***C*** assumes sole occurrence of the elementary Process 2, similar to limiting case ***B***, but now it starts only after limiting case ***A*** has been finished, *i.e.*, the starting sublayer-thickness values are $s_{\varepsilon,A}$ and $s_{\gamma',A}$, and the starting constant nitrogen concentration of the ε-sublayer is $y^{\varepsilon}_{\mathrm{eq}}$. The relation between the ε- and γ'-layer thicknesses in this case reads

$$s_\varepsilon = s_{\varepsilon,A} - \frac{(s_{\gamma'} - s_{\gamma',A}) V^{\varepsilon}_{y^{\varepsilon}_{\mathrm{eq}}}}{4\, y^{\varepsilon}_{\mathrm{eq}}\, V^{\gamma'}} \qquad [11]$$

The completion of boundary process ***C*** leads to the single γ'-layer with thickness $s_{\gamma',C} = s_{\gamma',B}$ (Eq. [10]).

The boundary processes ***A, B***, and ***C*** are represented in Figure 3 by the plotting of s_ε *vs* $s_{\gamma'}$.** For a mixed occurrence of the different subprocesses, the experimental values of $s_\varepsilon(s_{\gamma'})$ should fall within the "triangle" enclosed by the lines representing the limiting cases in Figure 3.

Note that, for the limiting cases ***A* and ***B***, s_ε depends only approximately linearly on $s_{\gamma'}$. Nonlinearity is introduced by the $y^{\varepsilon}_{\mathrm{av}}$-dependence of $V^{\varepsilon}_{y^{\varepsilon}_{\mathrm{av}}}$ for both cases (Eqs. [6] and [7]), and, in particular, for case ***B***, by the $s_{\gamma'}$ dependence of $y^{\varepsilon}_{\mathrm{av}}$, due to the concentration gradient in the ε-layer (Eq. [8] and its consequence for Eq. [7]).

V. EXPERIMENTAL RESULTS

A. *Optical Microscopy*

A typical ε/γ'-compound layer of an as-nitrided and quenched specimen*** is shown in Figure 4(a). Upon anneal-

***In spite of the identical nitriding conditions employed for all samples, the measured values of $s_{\varepsilon,0}$ and $s_{\gamma',0}$ vary slightly from specimen to specimen. Thus, the $s_{\varepsilon,0}$ and $s_{\gamma',0}$ are somewhat different for each annealing temperature.

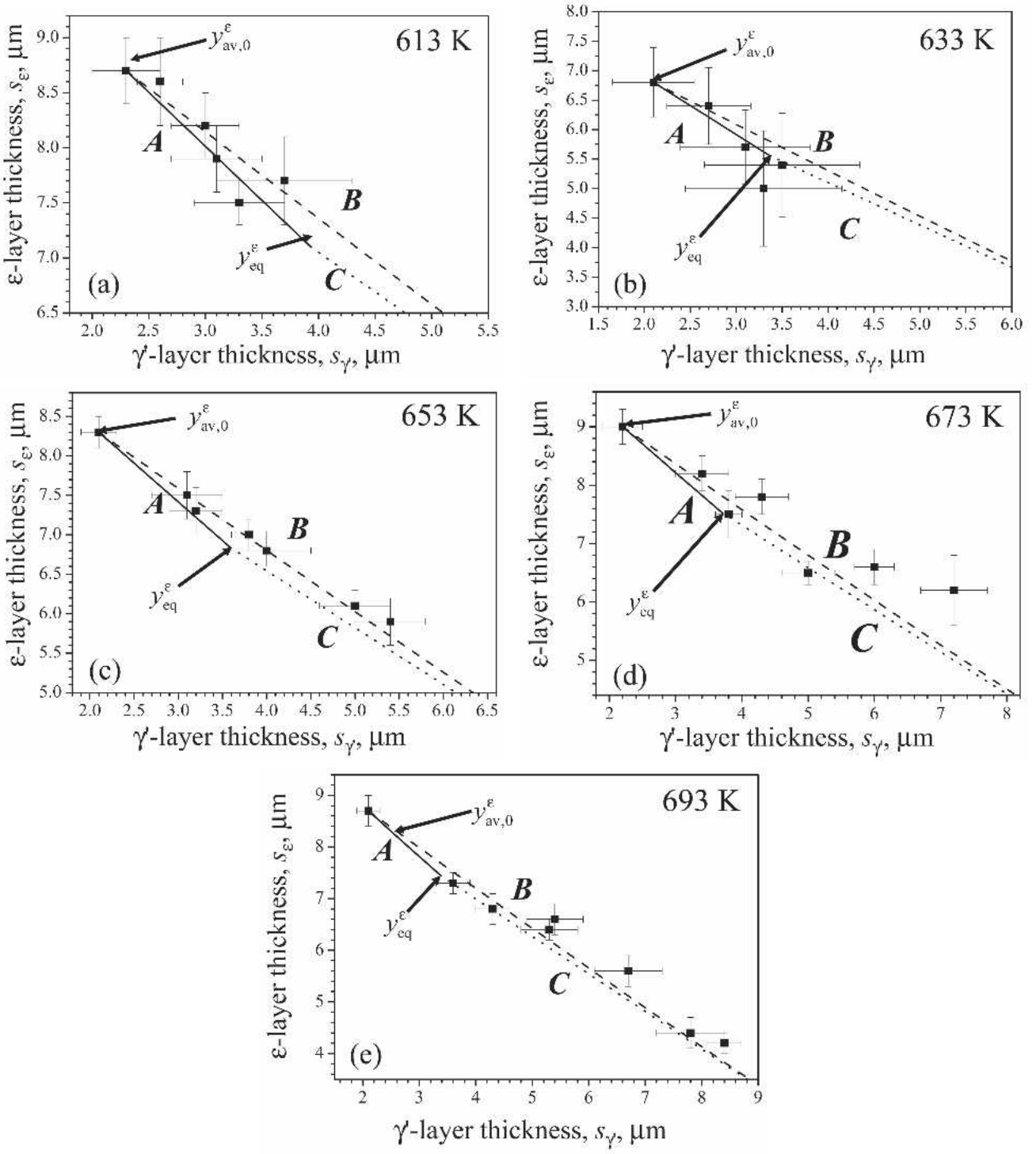

Fig. 3—Calculated plots of the sublayer thickness s_ε *vs* $s_{\gamma'}$, to illustrate the evolution of the ε- and γ′-layer thicknesses for the limiting cases ***A*** (solid line), ***B*** (dashed line), and ***C*** (dotted line). Experimental values, as determined by optical microscopy, are also shown. Note that information on the time dependences of s_ε and $s_{\gamma'}$ is lost by this presentation; that information is given in Fig. 5.

ing, layer-thickness changes occur, indicating that N redistribution takes place, as discussed in Section III (an increase in the γ′-sublayer thickness and a decrease in the ε-sublayer thickness, as in Figure 4(b)). Long-time annealing (40 days at 693 K, as in Figure 4(c)) leads to the complete disappearance of the ε-sublayer, *i.e.*, a single γ′-layer remains, which corresponds to the completion of limiting case ***B*** or limiting case ***C***. The thickness of the remaining single γ′-layer agrees with the predicted (Eq. [10]) value, within experimental accuracy (measured value: 14.2 (±0.8) μm; predicted value: 13.3 μm), thereby validating the mass balance considerations developed in Sections III and IV.

The evolution of the ε- and γ′-sublayer thicknesses, as determined by the optical microscopy of the cross sections

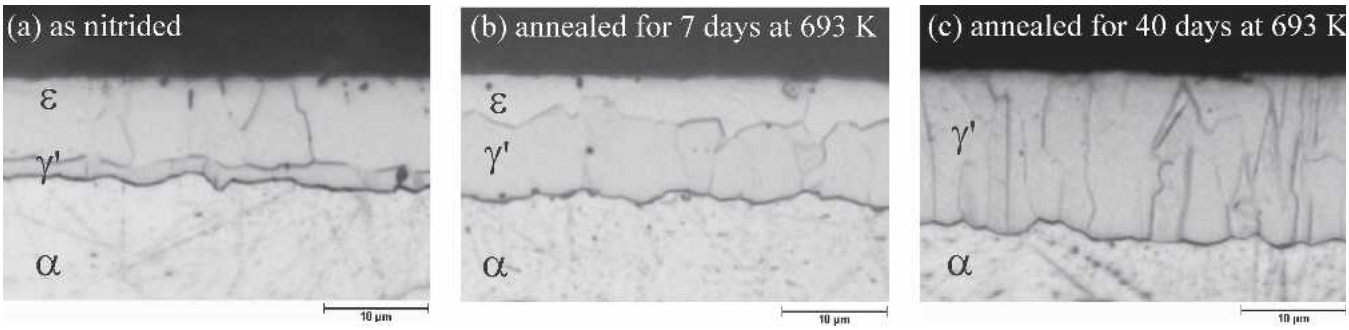

Fig. 4—Evolution of the compound layer (composed of ε- and γ'-iron nitride sublayers) on top of α-iron, upon annealing after nitriding: (*a*) as-nitrided and quenched iron specimen, (*b*) annealed for 7 days at 693 K, and (*c*) annealed for 40 days at 693 K.

(Section II), is presented in Figure 5 for each annealing temperature as a function of annealing time. For all temperatures investigated, the γ'-sublayer thickness increases and the ε-sublayer thickness decreases upon annealing.

At low annealing temperatures, the double-layer thickness remains constant, within experimental accuracy. According to the calculated results discussed in Section III, this would be compatible with the sole occurrence of Processes 1(a) and 1(b) (Figure 2). A virtually constant double-layer thickness does not necessarily exclude the occurrence of Process 2: for example, if the experimentally observed increase of the γ'-sublayer thickness, as observed for the 613 K data after 7 days of annealing (Figure 5), is attributed to occurrence of limiting case ***B*** (*i.e.*, Process 2, as in Sections III and IV), an increase in the double-layer thickness, $s_\varepsilon + s_{\gamma'}$, of only 0.3 μm is calculated, which is close to the accuracy of the microscopic layer-thickness determination (about 0.2 μm). Thus, additional information (about nitrogen concentration-profile development) is required, in order to reveal which processes are responsible for the observed layer-thickness changes; such data are obtained by analysis of the XRD data (Section V).

At higher annealing temperatures, Process 2 undoubtedly plays a role, because both the ε- and γ'-sublayer thicknesses cross (by the ε-sublayer thickness decrease and the γ'-sublayer increase) the values, $s_{\varepsilon,A}$ and $s_{\gamma',A}$, (dashed lines in Figure 5), which are calculated for the sole occurrence of Processes 1(a) and 1(b). Furthermore, the (total) double-layer thickness significantly increases, indicating the occurrence of Process 2.

The experimental data points plotted in an s_ε *vs* $s_{\gamma'}$ fashion (Figure 3) should be located within the triangle enclosed by the limiting cases, as discussed in Section IV; within the range of estimated standard deviations of s_ε and $s_{\gamma'}$, this is the case for the annealing temperatures investigated. Although the scatter of the experimental data due to experimental error in s_ε and $s_{\gamma'}$ is too large to be able to arrive at definitive conclusions about the preferential occurrence of either Process 1(a), 1(b), or 2 from only the s_ε *vs* $s_{\gamma'}$ plots, the experimental data validate the assumption of a constant amount of N in the whole compound layer, which was made in the calculations; this is the premise for the construction of the triangle enclosed by the three limiting cases in Figure 3. Hence, during annealing, the compound layer neither loses a significant amount of nitrogen (*e.g.*, by desorption to the atmosphere, as is also not expected to occur for the applied range of annealing temperatures[15,16]) nor gains a significant amount of nitrogen (*e.g.*, from the ferrite substrate).

B. *The XRD Results*

A comparison of the different diffraction patterns recorded (Section II) from an as-nitrided sample and a specimen cut from this sample and annealed at 693 K for 7 days and for 40 days (Figure 6), leads to the following conclusions: (1) shifts of the reflections of the ε-phase occur to lower diffraction angles upon annealing. This indicates the expected increase in N content in the ε-phase (Processes 1(b) and 2; Figure 2) (for the lattice parameters of ε as function of nitrogen content, refer to Reference 17); (2) narrowing of the reflections of the ε-phase occurs upon annealing. This is compatible with a leveling (homogenization) of the N concentration within the ε-phase[18] (Processes 1(a), 1(b), and 2; Figure 2); (3) the reflections of the ε-phase disappear after long-time annealing at 693 K, in agreement with the microscopic observations (Figure 4(c)) and the predictions for Processes 1(b) and 2.

For the lowest (613 K) and highest (693 K) annealing temperatures applied, the lattice-parameter values of the ε-phase, a^ε and c^ε, were extracted from the XRD data. It turned out that employing the fitted individual values of a^ε and c^ε to calculate the average N content of the ε-sublayer, $y^\varepsilon_{\text{av}}$ (from a^ε) and $y^\varepsilon_{\text{av}}$ (from c^ε), using Eqs. [A3] and [A4], respectively, led to significantly different values for the average nitrogen concentration in the ε-phase. In fact, the $c^\varepsilon/a^\varepsilon$ lattice-parameter ratios are too large for ε-iron nitrides in the expected range of composition.[17] This apparent anomaly can be due to the following:

(a) The fact that the compound layer probably exhibits macrostresses, which, furthermore, are depth dependent.[19] In combination with the unknown and likely anisotropic elastic compliance of the iron nitrides, in particular for the ε-phase, this can lead to considerable deviations in the measured lattice parameters from their stress-free equilibrium values.
(b) Negligence of the presence of a nonconstant N concentration depth profile in the ε-sublayer, in particular for the as-nitrided sample (Figure 2). In view of the absorption of CoK_α radiation in the ε-phase (note that the reciprocal of the linear absorption coefficient, $[\mu(\text{Co})]^{-1}$, equals about 30 μm, which is not much larger

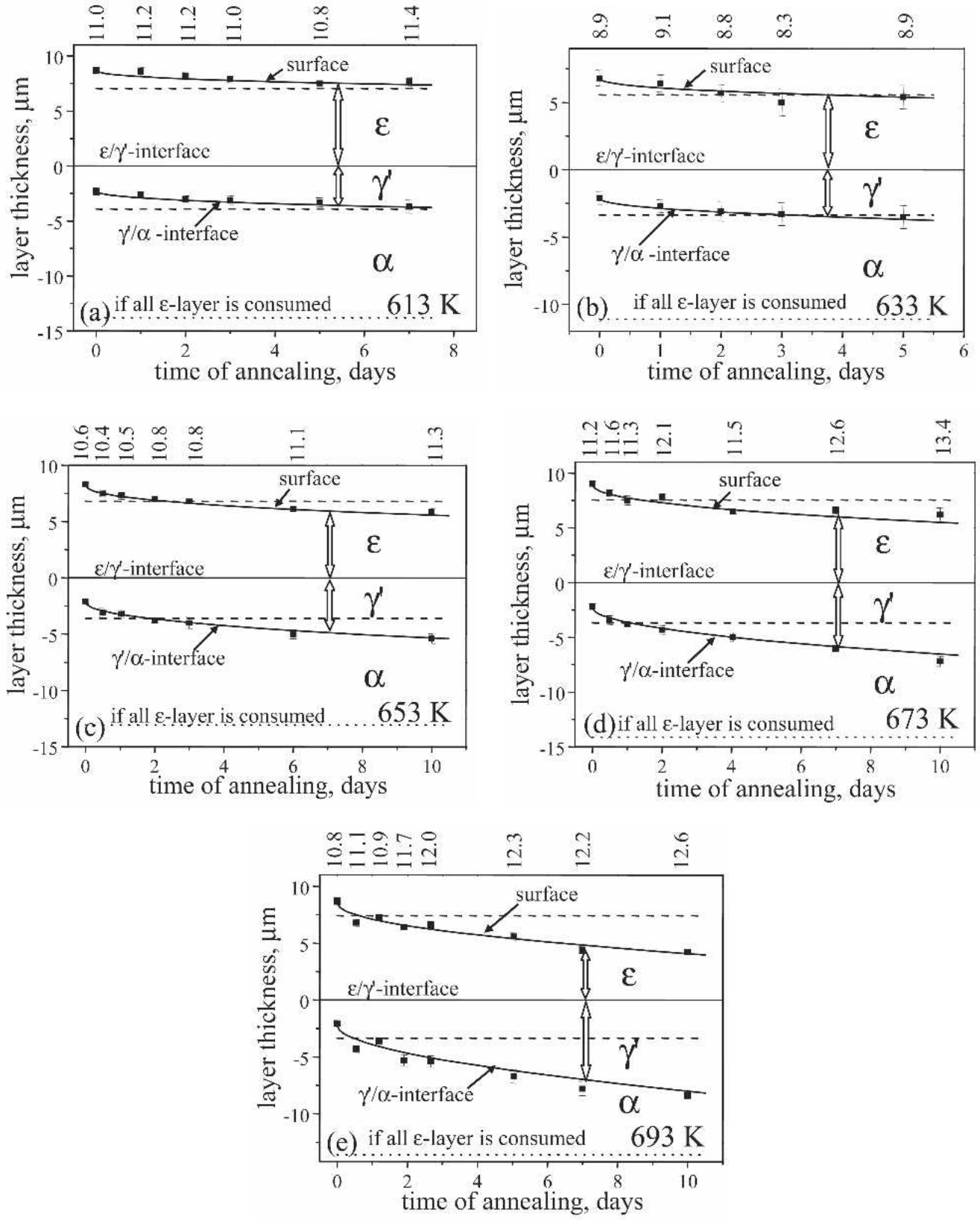

Fig. 5—Changes in the ε/γ'-iron-nitride sublayer thicknesses as a function of the annealing time at different annealing temperatures. The ε-sublayer thicknesses (s_ε) have been plotted as positive values and the γ'-sublayer thicknesses ($s_{\gamma'}$) have been plotted as negative values, by taking the depth of the ε/γ'-interface as reference (*i.e.*, depth = 0). The double-layer thickness, *i.e.*, the sum of the experimentally measured s_ε and $s_{\gamma'}$ values, has been given by the numbers (in μm) printed at the top of the diagram. The dashed lines show the final thicknesses of the ε/γ'-sublayers, if only Processes 1(a) and 1(b) operated (limiting case ***A***). The dotted lines represent the final γ'-layer thickness, when all ε-phase has been consumed. The simulated (on the basis of fitted volume diffusion coefficients, as discussed in Section VI) time-dependent behaviors of the ε/γ'-sublayer thicknesses upon annealing are shown by the solid curves.

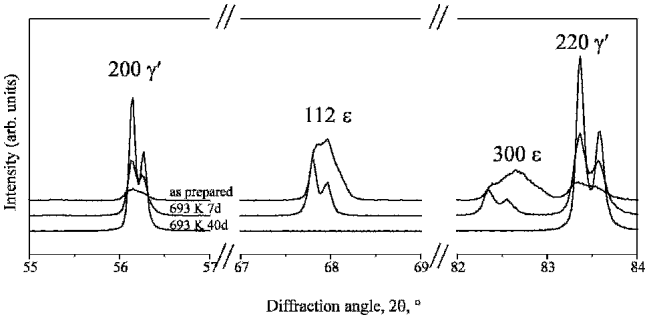

Fig. 6—The XRD patterns (with zero-intensity level shifted with respect to each other) for the as-prepared sample, and the annealed (for 7 days) and long-time annealed (40 days) samples at 693 K.

than s_ε), the y values obtained from the XRD data are not necessarily equal to y^ε_{av}.

In view of the complications just described under (a) and (b), the XRD data can only be used as a qualitative indication of the evolution of an average N content, $y^\varepsilon_{av,XRD}$:

$$y^\varepsilon_{av,XRD} = (2y^\varepsilon_{av}(a^\varepsilon) + y^\varepsilon_{av}(c^\varepsilon))/3 \qquad [12]$$

which expresses the relative weights for the two N content levels obtained individually from a^ε and c^ε. The value of $y^\varepsilon_{av,XRD}$ has been plotted as a function of the annealing time, in Figure 7. The course of $y^\varepsilon_{av,XRD}$ upon the annealing can be compared with the evolutions of the averaged N content y^ε_{av}, as obtained from $y^\varepsilon_{av}(s_\gamma)$ and $y^\varepsilon_{av}(s_\varepsilon)$, calculated from the microscopically determined sublayer-thickness values s_ε and s_γ:

$$y^\varepsilon_{av} = y^\varepsilon_{av}(s_\varepsilon)/2 + y^\varepsilon_{av}(s_\gamma)/2 \qquad [13]$$

If the sole occurrence of limiting case ***A*** is assumed (*i.e.*, $y^\varepsilon_{av}(s_\gamma)$ and $y^\varepsilon_{av}(s_\varepsilon)$, as obtained by the application of Eqs. [5] and [6], respectively) or if the sole occurrence of limiting case ***B*** is assumed (*i.e.*, $y^\varepsilon_{av}(s_\gamma)$ and $y^\varepsilon_{av}(s_\varepsilon)$, as obtained by application of Eqs. [8] and [9], respectively), theoretical evolutions of y^ε_{av} are obtained, which have also been plotted in Figure 7.

A comparison of the experimental 613 K data for $y^\varepsilon_{av,XRD}$, as a function of annealing time, with the evolutions of y^ε_{av} calculated for the limiting cases ***A*** and ***B***, shows that only limiting case ***A*** likely describes reality (Figure 7(a)). This confirms the preliminary conclusion in Reference 6 that Processes 1(a) and 1(b) are dominating the N redistribution at low temperatures.

The significant increase in the double-layer thickness at 693 K (Figure 5(e)) indicates that the nitrogen redistribution at 693 K is certainly incompatible with the sole occurrence of limiting case ***A*** (Section V). According to the $y^\varepsilon_{av,XRD}$ data (Figure 7(b)), the increase in the average N content of the ε-layer is largely accomplished during the first 12 hours of annealing; the y^ε_{av} calculated for the sole occurrence of limiting case ***B***, on the other hand, indicates a more gradual increase in the N content. These results suggest that all the processes discussed for the observed layer-thickness changes (1(a), 1(b), and 2) predominantly take place at high annealing temperatures.

The results of the XRD analysis discussed earlier agree well with the results obtained by electron probe microanalysis (EPMA),[7] which revealed a leveling of the N content for

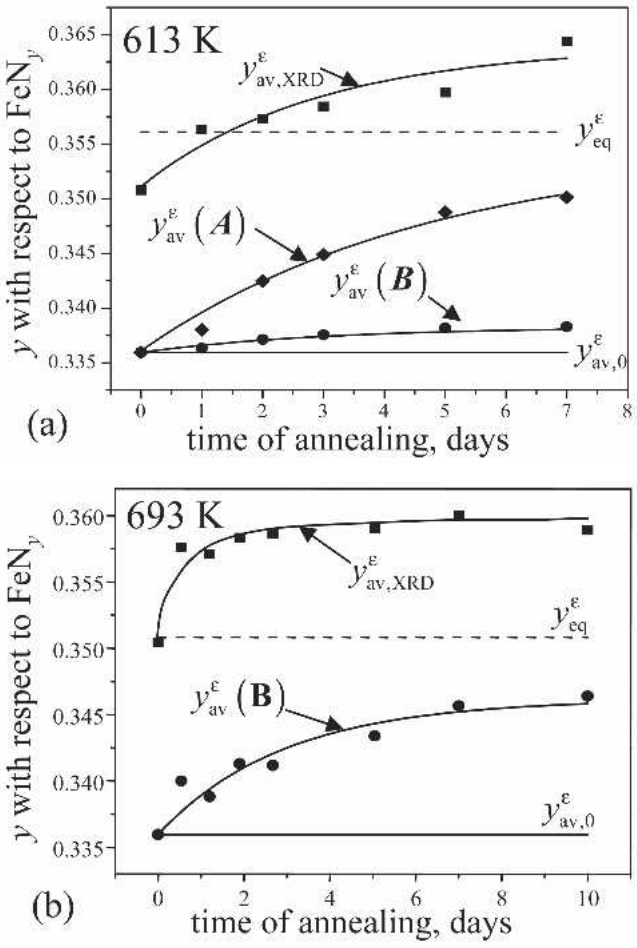

Fig. 7—Evolution of the averaged N content in the ε/γ′-compound layer occurring upon annealing at (*a*) 613 K and at (*b*) 693 K. The $y^\varepsilon_{av,XRD}$ data have been extracted from lattice parameters obtained from the X-ray powder-diffraction data (Eq. [12]). The theoretical y^ε_{av} data have been calculated from the microscopically determined layer thicknesses s_ε and s_γ for the limiting case ***A*** (at 693 K, the limiting case ***A*** can be excluded, due to the observed significant increase in the double-layer thickness) and for the limiting case ***B***, using Eq. [13]. The drawn curves serve as guides for the eyes. The average initial N content in the as-nitrided sample, $y^\varepsilon_{av,0}$, and the equilibrium N concentration for the corresponding annealing temperature, y^ε_{eq}, have been indicated by solid and dashed lines, respectively.

Process 1(a), and an increase in the N content for Process 1(b), in the ε-layer at different annealing temperatures, as well as an acceleration of these processes with an increase in the annealing temperature.

It can be concluded that, at relatively low annealing temperatures, Processes 1(a) and 1(b) dominate the N redistribution, whereas at relatively high annealing temperatures, all processes play a role; Processes 1(a) and 1(b) are accomplished quickly, as compared to Process 2 (as evidenced by the increase in the average N content in the ε-sublayer and by the sublayer-thickness changes, respectively).

VI. SIMULATION OF THE N REDISTRIBUTION KINETICS

In this section, the microscopically determined separate time dependencies of s_ε and s_γ at the different annealing

temperatures (Section V) are used to determine the diffusion coefficients of N in the ε-phase and the γ'-phase. To this end, a kinetic model was developed, which has the following bases.

(a) All three processes (1(a), 1(b), and 2) (may) occur simultaneously.
(b) Local equilibrium holds at all interfaces.
(c) Nitrogen redistribution occurs through the volume diffusion of nitrogen.

The nitrogen concentration-profile development in the ε-phase, as due to the volume diffusion of nitrogen (Processes 1(a) and 1(b)), is described by Fick's second law:

$$\frac{\partial c_{\mathrm{N}}^{\varepsilon}}{\partial t} = D_{\mathrm{N}}^{\varepsilon} \frac{\partial^2 c_{\mathrm{N}}^{\varepsilon}}{\partial s^2} \qquad [14]$$

where $D_{\mathrm{N}}^{\varepsilon}$ is the intrinsic diffusion coefficient of N in the ε-phase, which has been taken as independent of the concentration, in the (relatively small) range of N concentration considered (Figure 7); $c_{\mathrm{N}}^{\varepsilon}$ is the molar concentration of N; and t is the time. Because $\partial c_{\mathrm{N}}^{\varepsilon} = \partial y^{\varepsilon}/(N_{\mathrm{A}} V^{\varepsilon})$, where N_{A} is Avogadro's constant, Eq. [14] can be expressed in terms of y, as follows:

$$\frac{\partial y^{\varepsilon}}{\partial t} = D_{\mathrm{N}}^{\varepsilon} \frac{\partial^2 y^{\varepsilon}}{\partial s^2} \qquad [15]$$

The nitrogen flux through the γ'-layer, $J_{\mathrm{N}}^{\gamma'}$ (Process 2), is described by Fick's first law, given here as

$$J_{\mathrm{N}}^{\gamma'} = -D_{\mathrm{N}}^{\gamma'} \frac{\Delta c_{\mathrm{N}}^{\gamma'}}{s_{\gamma'}} \qquad [16]$$

where $D_{\mathrm{N}}^{\gamma'}$ is the effective diffusion coefficient* of nitrogen for diffusion through the γ'-phase, with a homogeneity range of $\Delta c_{\mathrm{N}}^{\gamma'}$ at the annealing temperature. Substituting $\Delta c_{\mathrm{N}}^{\gamma'} = \Delta y^{\gamma'}/(N_{\mathrm{A}} V^{\gamma'})$ yields

$$J_{\mathrm{N}}^{\gamma'} = -D_{\mathrm{N}}^{\gamma'} \frac{\Delta y^{\gamma'}}{N_A V^{\gamma'} s_{\gamma'}} \qquad [17]$$

The γ'-phase has a very narrow composition range $\Delta y^{\gamma'}$, which is not precisely known, in particular, at relatively low temperatures. To handle this problem, a so-called integral diffusion coefficient,[20] $D_{\mathrm{N,int}}^{\gamma'} = D_{\mathrm{N}}^{\gamma'} \Delta y^{\gamma'}$ can be adopted to describe the flux through the γ'-phase

$$J_{\mathrm{N}}^{\gamma'} = -D_{\mathrm{N,int}}^{\gamma'} \frac{1}{N_{\mathrm{A}} V^{\gamma'} s_{\gamma'}} \qquad [18]$$

On this basis, an algorithm has been developed for the numerical simulation of the evolution of the concentration-depth profile, departing from a given starting profile (Section III) and given values of $D_{\mathrm{N,int}}^{\gamma'}$ and $D_{\mathrm{N}}^{\varepsilon}$. This algorithm applies the finite-difference method and allows for moving interfaces,[24,25] and is described in detail in Reference 26. An example of the simulated time-dependent evolution of a certain concentration-depth profile is depicted in Figure 8.

*The effective diffusion coefficient for diffusion through the γ'-phase is the composition-weighted average of the intrinsic diffusion coefficient over the homogeneity range of the γ'-phase; for example, Ref. 3.

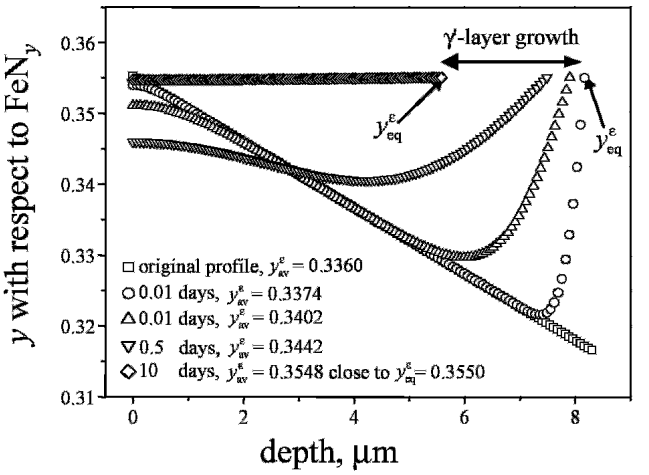

Fig. 8—Simulated nitrogen-concentration profile in the ε-phase, for different annealing times at 653 K using the $D_{\mathrm{N}}^{\varepsilon}$ and $D_{\mathrm{N,int}}^{\gamma'}$, as obtained by comparison of the observed and simulated time-dependences of the sublayer thicknesses.

The algorithm described has been implemented into a nonlinear least-squares fitting algorithm, employed to obtain for a given annealing temperature $D_{\mathrm{N,int}}^{\gamma'}$ and $D_{\mathrm{N}}^{\varepsilon}$, on the basis of a comparison of the observed and the simulated evolutions of s_{ε} and $s_{\gamma'}$, by minimizing the sum of squared differences, χ^2:

$$\chi^2 = \sum \left(s_{\gamma'}^{\mathrm{calc}} - s_{\gamma'}^{\mathrm{exper}}\right)^2 + \sum \left(s_{\varepsilon}^{\mathrm{calc}} - s_{\varepsilon}^{\mathrm{exper}}\right)^2 \qquad [19]$$

At the lowest temperature (613 K), Process 2 plays a marginal role and the concentration-profile evolution is dominated by Processes 1(a) and 1(b), which are controlled by $D_{\mathrm{N}}^{\varepsilon}$. At the relatively high temperature (693 K), Processes 1(a) and 1(b) are completed very fast and then the concentration profile-evolution is dominated by Process 2, which is controlled by $D_{\mathrm{N,int}}^{\gamma'}$ (Section V). Therefore, the fitting of both $D_{\mathrm{N}}^{\varepsilon}$ and $D_{\mathrm{N,int}}^{\gamma'}$ has been performed for the intermediate annealing temperatures of 633, 653, and 673 K. The resulting values for the diffusion coefficients have been plotted in Figure 9 in an Arrhenius-type fashion, resulting in values for the activation energies (Q) and the pre-exponential factors (D_0) (*i.e.*, $\ln D = \ln D_0 - Q/\mathrm{R}T$) according to

$$\ln[D_{\mathrm{N}}^{\varepsilon}/(\mathrm{m}^2\mathrm{s}^{-1})] = -15.6(\pm 5.0) - 118(\pm 30)\ \mathrm{kJ\ mol^{-1}}/(\mathrm{R}T) \qquad [20]$$

and

$$\ln[D_{\mathrm{N,int}}^{\gamma'}/(\mathrm{m}^2\mathrm{s}^{-1})] = -20.5(\pm 0.6) - 116(\pm 30)\ \mathrm{kJ\ mol^{-1}}/(\mathrm{R}T) \qquad [21]$$

for the applied range of annealing temperatures.

The corresponding simulated time dependencies of the ε/γ'-layer thicknesses are shown in Figure 5, together with the experimentally determined thickness values. Evidently, good fits are possible on the basis of the volume diffusion as the rate-controlling transport mechanism. Next, the evolutions of s_{ε} and $s_{\gamma'}$ at 613 and 693 K were simulated using the now-determined diffusion coefficients, $D_{\mathrm{N}}^{\varepsilon}$ and $D_{\mathrm{N,int}}^{\gamma'}$, respectively (Eqs. [20] and [21]). These evolutions are also shown in Figure 5. Again, simulated and experimental data agree well.

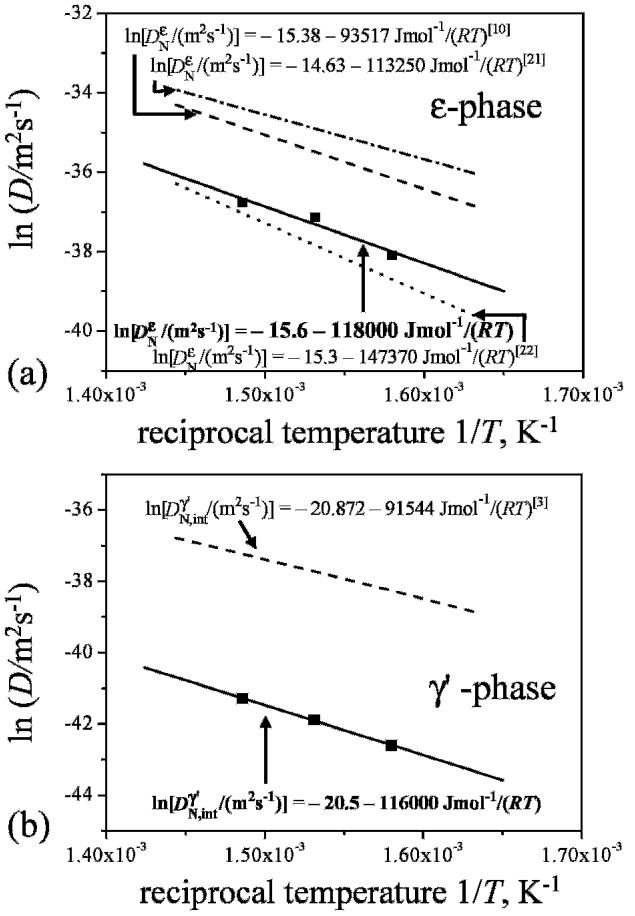

Fig. 9—Arrhenius plots for (*a*) the intrinsic diffusion coefficient of the ε-phase, D_N^ε, and (*b*) the integral diffusion coefficient of the γ'-phase, $D_{N,int}^{\gamma'}$. The data points have been obtained by model fits to sublayer-thickness data obtained at relatively low temperatures. The dashed, dotted, and dashed-dotted lines represent extrapolations using expressions given in the literature or expressions obtained here by fitting to values given in the literature, all based on experiments at significantly higher temperatures.

VII. DISCUSSION

For metal-interstitial (*e.g.*, nitrogen and carbon) systems, the most commonly applied method for studying the long-range diffusion processes of interstitials and the associated phase transformations is the exposure of the metal to an environment (*e.g.*, a gas phase) with a usually constant activity of the light element. Especially if the nitride or carbide surface layers grow, the inward diffusion of the light element can be traced by the time- and temperature-dependent compound-layer thicknesses.

Numerous experimental and theoretical studies have been reported related to the inward diffusion of nitrogen into iron, generating compound layers at the surface.[3,8,9,21,22,27–36] The evaluation of the N mobility is usually based on the time- and temperature-dependent γ'- or ε/γ'-layer-thicknesses. Various methods have been developed, or standard methods have been adapted, to these processes, in order to determine diffusion coefficients from the kinetic data. However, the determined diffusion coefficients, as obtained from the different studies, cannot always straightforwardly be compared with each other, because the models employed for the diffusion kinetics underlying the determination of the diffusion coefficients are often incompatible (*e.g.*, concerning the concentration dependences of the diffusion coefficients or the phase-boundary concentrations).

The concepts applied previously to describe the kinetics of the inward diffusion of nitrogen into iron through a compound layer on the surface cannot on their own be used for the experiments presented here, which deal with N redistribution processes occurring in compound layers upon annealing; an additional supply of nitrogen from the gas phase must be taken into account. This concerns, in particular, the ε-sublayer, in which relatively complicated concentration-depth profiles are expected to develop upon low-temperature annealing, due to the temperature dependence of the nitrogen concentration in ε at the phase-boundary concentration in contact with the γ'-phase, y_{eq}^ε.

The data obtained in this work for D_N^ε and $D_{N,int}^{\gamma'}$ should be compared with data from the literature, in which similarly defined diffusion coefficients have been employed for the data evaluation. In this context, it should be noted not only that the values from the literature were all obtained from N-inward-diffusion experiments, but also that these experiments were conducted above 800 K, *i.e.*, a comparison involves extrapolation of the data from the literature over a considerable temperature range, since the present experiments were performed below 700 K.

Suitable (in the sense indicated earlier) values from the literature for D_N^ε were obtained from References 9, 21, and 22, and have been indicated in Figure 9(a). Also, in view of the significant differences between the previous data from the literature for D_N^ε, the presently obtained values can be regarded as reasonable in light of the other data. The presently determined values of $D_{N,int}^{\gamma'}$ can be compared with the integral diffusion coefficients calculated from the tabulated (temperature-dependent) tracer diffusion coefficients, from the thermodynamic factors, and from the values for the phase width $\Delta y^{\gamma'}$[3] (Figure 9(b)). The currently obtained diffusion coefficients are significantly smaller than the values obtained from Reference 3. Furthermore, the activation energy determined here (about 115 kJ/mol) is higher than the value from Reference 3 (91.5 kJ/mol).

It should be recognized that the accuracy of the present analysis depends not only on experimental errors but also on possible uncertainties. One problem may be the N content of the ε-phase in equilibrium with the γ'-phase, which was taken from the review given in Reference 3. It may also be argued that the assumption of local equilibrium at the phase interfaces may not hold. However, the good fits obtained on the basis of the volume diffusion model seem to exclude this.

VIII. CONCLUSIONS

Annealing ε/γ'-iron nitride compound layers on α-iron substrates at relatively low temperatures in the range of 613 to 693 K (significantly lower than the nitriding temperature (823 K)) leads to various ways of redistributing N in the compound layer:

1. The leveling of the initial N concentration gradient in the ε-layer;
2. The backward growth of the γ'-layer into the ε-layer, thereby increasing the N content in the ε-layer; and

3. The reaction of N from the ε-layer, with ferrite beneath the γ'-layer forming new γ'-phase at both the ε/γ'-interface and the γ'/α-interface, leading, finally, to a single γ'-layer on top of the ferrite substrate.

The observed time dependences of the sublayer-thickness changes can be well modeled, assuming the volume diffusion of N within the γ'- and ε-phases as the rate-determining transport mechanism. The diffusion coefficients of N in the ε- and γ'-phases, as obtained from the nonlinear least-squares fitting of the model to the experimental data, are given by

$$\ln[D_{\mathrm{N}}^{\varepsilon}/(\mathrm{m}^2\mathrm{s}^{-1})] = -15.6 - 118\ \mathrm{kJ\ mol}^{-1}/(\mathrm{R}T)$$

and

$$\ln[D_{\mathrm{N,int}}^{\gamma'}/(\mathrm{m}^2\mathrm{s}^{-1})] = -20.5 - 116\ \mathrm{kJ\ mol}^{-1}/(\mathrm{R}T).$$

APPENDIX

Mass-balance considerations

All mass-balance considerations concerning the redistribution processes of nitrogen are based on the conservation of the number of nitrogen atoms in the compound layer, which is for a given area A, parallel to the surface of the layer, as follows:

$$\frac{N_{\mathrm{N}}}{A} = \int_0^{s_\varepsilon+s_{\gamma'}} \frac{y(s)}{V_{y(s)}^{\varphi}}\,ds = \frac{N_{\mathrm{N}}^{\varepsilon}}{A} + \frac{N_{\mathrm{N}}^{\gamma'}}{A} = \int_0^{s_\varepsilon} \frac{y^{\varepsilon}(s)}{V_{y^{\varepsilon}(s)}^{\varepsilon}}\,ds + \int_{s_\varepsilon}^{s_\varepsilon+s_{\gamma'}} \frac{y^{\gamma'}(s)}{V_{y^{\gamma'}(s)}^{\gamma'}}\,ds \qquad [A1]$$

where integration over the depth (measured from the surface) is performed, considering the sublayers separately, from 0 to s_ε for the ε-phase sublayer ($\varphi = \varepsilon$) and from s_ε to $s_\varepsilon + s_{\gamma'}$ for the γ'-phase ($\varphi = \gamma'$). The y is the nitrogen content with respect to the formula FeN_y; $V_{y(s)}^{\varphi}$ is the y-dependent volume per iron atom (*i.e.*, the volume per unit cell divided by the number of iron atoms in the unit cell) of that iron-nitride phase φ, which is present in the compound layer at the depth s.

The number of iron atoms in the compound layer is analogously

$$\frac{N_{\mathrm{Fe}}}{A} = \int_0^{s_\varepsilon+s_{\gamma'}} \frac{1}{V_{y(s)}^{\varphi}}\,ds = \int_0^{s_\varepsilon} \frac{1}{V_{y^{\varepsilon}(s)}^{\varepsilon}}\,ds + \int_0^{s_\varepsilon+s_{\gamma'}} \frac{1}{V_{y^{\gamma'}(s)}^{\gamma'}}\,ds \qquad [A1a]$$

The γ'-$\mathrm{Fe_4N}$ phase is considered to be stoichiometric with $y^{\gamma'} = 1/4$ ($\mathrm{FeN}_{1/4}$), having a volume per iron atom for $y^{\gamma'} = 1/4$, according to Reference 23, as follows:

$$V_{y^{\gamma'}}^{\gamma'} = \left(a^{\gamma'}\right)^3/4 = 13.705\ \text{Å}^3 \qquad [A2]$$

where $a^{\gamma'}$ is the cubic lattice parameter of the γ'-phase.

The ε-phase can vary considerably in composition. The lattice parameters, a_ε and c_ε, of the hexagonal ε-phase, depend on N content and are given by (as applicable to quenched ε-iron nitride)[17]

$$a^{\varepsilon}(\text{Å}) = 4.4542 + 0.7111\,y^{\varepsilon} \qquad [A3]$$

$$c^{\varepsilon}(\text{Å}) = 4.2535 + 0.3662\,y^{\varepsilon} \qquad [A4]$$

Since the unit cell of the ε-phase contains six Fe atoms, the volume per iron atom is given by

$$V_{y^{\varepsilon}(s)}^{\varepsilon}\left(\text{Å}^3\right) = \sqrt{3}/12\left(a^{\varepsilon}\right)^2 c^{\varepsilon} \qquad [A5]$$

For an inhomogeneous ε-phase sublayer (y^{ε} depends on the depth variable s_ε), the amounts of N and Fe atoms can be approximately calculated by

$$\frac{N_{\mathrm{N}}^{\varepsilon}}{A} = \int_0^{s_\varepsilon} \frac{y^{\varepsilon}(s)}{V_{y^{\varepsilon}(s)}^{\varepsilon}}\,ds \approx \frac{y_{\mathrm{av}}^{\varepsilon}\,s_\varepsilon}{V^{\varepsilon}(y_{\mathrm{av}}^{\varepsilon})} \qquad [A6]$$

and

$$\frac{N_{\mathrm{Fe}}^{\varepsilon}}{A} = \int_0^{s_\varepsilon} \frac{1}{V_{y^{\varepsilon}(s)}^{\varepsilon}}\,ds \approx \frac{s_\varepsilon}{V^{\varepsilon}(y_{\mathrm{av}}^{\varepsilon})} \qquad [A7]$$

where $y_{\mathrm{av}}^{\varepsilon} = \left(y_{\mathrm{gas}/\varepsilon}^{\varepsilon} + y_{\varepsilon/\gamma'}^{\varepsilon}\right)/2$ is the average N content in the ε-phase sublayer, adopting a linear concentration-depth profile in the ε-sublayer (Section III). One can show, by comparison of the outcomes of Eqs. [A1] and [A1a] with the outcomes of Eqs. [A6] and [A7], that the exact and approximate results are practically the same. Equations [A6] and [A7] indicate that, irrespective of the distribution of nitrogen within the ε-phase, its thickness depends only on $y_{\mathrm{av}}^{\varepsilon}$ and on the absolute number of Fe atoms per unit area (parallel to the surface of the layer) inside the ε-phase.

REFERENCES

1. *Source Book on Nitriding*, ASM, Metals Park, OH, 1977.
2. R. Chatterjee-Fischer *et al.*: *Wärmebehandlung von Eisenwerkstoffen. Nitrieren und Nitrocarburieren*, Expert-Verlag, Renningen-Malmsheim, Germany, 1995.
3. E.J. Mittemeijer and M.A.J. Somers: *Surface Eng.*, 1997, vol. 13, pp. 483-97.
4. H.A. Wriedt, N.A. Gokcen, and R.H. Nafziger: *Bull. Alloy Phase Diagrams*, 1987, vol. 8, pp. 355-77.
5. S. Malinov, A.J. Böttger, E.J. Mittemeijer, M.I. Pekelharing, and M.A.J. Somers: *Metall. Mater. Trans. A*, 1995, vol. 32A, pp. 59-73.
6. T. Liapina, A. Leineweber, and E.J. Mittemeijer: *Scripta Mater.*, 2003, vol. 48, pp. 1643-48.
7. T. Liapina, A. Leineweber, and E.J. Mittemeijer: *Defect Diff. Forum*, 2005, vols. 237–240, pp. 1147-52.
8. M.A.J. Somers and E.J. Mittemeijer: *Metall. Mater. Trans. A*, 1995, vol. 26A, pp. 57-74.
9. L. Torchane, P. Bilger, J. Dulcy, and M. Gantois: *Metall. Mater. Trans. A*, 1996, vol. 27A, pp. 1823-35.
10. M.A.J. Somers and E.J. Mittemeijer: *Metall. Trans. A*, 1990, vol. 21A, pp. 901-12.
11. W. Schröter, R. Russev, K. Ibendorf, and E. Vatev: *Wiss. Z. Techn. Hochsch. Karl-Marx-Stadt*, 1982, vol. 24, pp. 786-94.
12. D. Gerardin, J. Morniroli, H. Michel, and M. Gantois: *J. Mater. Sci.*, 1981, vol. 16, pp. 159-69.
13. E.J. Sonneveld and R. Delhez: *ProFit*, Version 1.0c, Philips Electronics NV, 1996.
14. L. Małdziński, Z. Przyłecki, and J. Kunze: *Steel Res.*, 1986, vol. 57, pp. 645-49.
15. C.F. Goodeve and K.H. Jack: *Disc. Faraday Soc.*, 1948, vol. 4, pp. 82-91.
16. A. Leineweber, H. Jacobs, F. Hüning, H. Lueken, and W. Kockelmann: *J. Alloys Compounds*, 2001, vol. 316, pp. 21-38.
17. T. Liapina, A. Leineweber, E.J. Mittemeijer, and W. Kockelmann: *Acta Mater.*, 2004, vol. 52, pp. 173-80.
18. A. Leineweber and E.J. Mittemeijer: *J. Appl. Crystallogr.*, 2004, vol. 37, pp. 123-35.
19. M.A.J. Somers and E.J. Mittemeijer: *Metall. Trans. A*, 1990, vol. 21A, pp. 189-204.
20. C. Wagner: *Acta Metall.*, 1969, vol. 17, pp. 99-107.
21. B. Prenosil: *Kovove Mater.*, 1965, vol. 3, pp. 69-87.
22. Y.M. Lakhtin and Y.D. Kogan: *Nitriding of Steel*, Mashinostroenie, Moscow, 1976.

23. M.A.J. Somers, N.M. van der Pers, D. Schalkoord, and E.J. Mittemeijer: *Metall. Trans. A*, 1989, vol. 20A, pp. 1533-39.
24. J. Crank: *The Mathematics of Diffusion*, Clarendon, Oxford, United Kingdom, 1975.
25. J. Crank: *Free and Moving Boundary Problems*, Clarendon, Oxford, United Kingdom, 1987.
26. T. Liapina: Ph.D. Thesis, University of Stuttgart, Stuttgart, 2005.
27. M. Keddam, M.E. Djeghlal, and L. Barrallier: *Appl. Surf. Sci*., 2005, vol. 242, pp. 369-74.
28. M. Keddam, M.E. Djeghlal, L. Barrallier, and E. Salhi: *Comp. Mater. Sci*., 2004, vol. 29, pp. 43-48.
29. M.A.J. Somers: *J. Phys. IV*, 2004, vol. 120, pp. 21-33.
30. J. Ratajski: *Z. Metallkd*., 2004, vol. 95, pp. 823-28.
31. T. Belmonte, M. Gouné, and H. Michel: *Mater. Sci. Eng. A*, 2001, vol. 302, pp. 246-57.
32. L. Maldzinski, W. Liliental, G. Tymowski, and J. Tacikowski: *Surf. Eng*., 1999, vol. 15, pp. 377-84.
33. H. Du and J. Ågren: *Z. Metallkd*., 1995, vol. 86, pp. 522-29.
34. C.-K. Chang: J.-Y. Lee, and S.Y. Kim: *J. Kor. Inst. Met*., 1979, vol. 17, pp. 455-67.
35. A. Marciniak: *Surf. Eng*., 1985, vol. 1, pp. 283-88.
36. W.D. Jentzsch and S. Böhmer: *Neue Hütte*, 1979, vol. 24, pp. 249-53.